Hindawi Publishing Corporation
Journal of Nanomaterials
Volume 2011, Article ID 853989, 7 pages
doi:10.1155/2011/853989

*Research Article*

# Pore-Width-Dependent Preferential Interaction of $sp^2$ Carbon Atoms in Cyclohexene with Graphitic Slit Pores by GCMC Simulation

**Natsuko Kojima,[1] Tomonori Ohba,[1] Yasuhiko Urabe,[2] Hirofumi Kanoh,[1] and Katsumi Kaneko[1,3]**

[1] *Graduate School of Science, Chiba University, 1-33 Yayoi, Inage, Chiba 263-8522, Japan*
[2] *Technology Development Devision, TOKYO GAS Co., Ltd., 2-7, Suehirocho 1, Tsurumiku, Yokohama 230-0045, Japan*
[3] *Research Center for Exotic NanoCarbon Project, Shinshu University, 4-17-1, Wakasato, Naganoshi 380-8553, Japan*

Correspondence should be addressed to Tomonori Ohba, ohba@pchem2.s.chiba-u.ac.jp

Received 2 June 2010; Accepted 1 November 2010

Academic Editor: Sulin Zhang



The adsorption of cyclohexene with two $sp^2$ and four $sp^3$ carbon atoms in graphitic slit pores was studied by performing grand canonical Monte Carlo simulation. The molecular arrangement of the cyclohexene on the graphitic carbon wall depends on the pore width. The distribution peak of the $sp^2$ carbon is closer to the pore wall than that of the $sp^3$ carbon except for the pore width of 0.7 nm, even though the Lennard-Jones size of the $sp^2$ carbon is larger than that of the $sp^3$ carbon. Thus, the difference in the interactions of the $sp^2$ and $sp^3$ carbon atoms of cyclohexene with the carbon pore walls is clearly observed in this study. The preferential interaction of $sp^2$ carbon gives rise to a slight tilting of the cyclohexene molecule against the graphitic wall. This is suggestive of a $\pi$-$\pi$ interaction between the $sp^2$ carbon in the cyclohexene molecule and graphitic carbon.

## 1. Introduction

There has been an increase in the use of activated carbons in the construction of environmentally friendly technologies with sufficient safety. Activated carbon has basically slit-shaped micropores, which provide much better accessibility for most molecules than the cylindrical pores of zeolites [1, 2]. Recent researches have succeeded in controlling the pore width in the range from subnanometers to several nanometers; this has resulted in improvements in a wide range of applications, such as air separation (or air purification), solvent recovery, and manufacture of automobile canisters [3–7]. Furthermore, activated carbons have high electronic conductivities, allowing them to be used in electrochemical applications such as supercapacitors [8–10]. Another striking advantage of activated carbons is the fact that their production from natural products that fix atmospheric $CO_2$ can contribute to $CO_2$ sequestration [5, 11, 12]. However, there are still many research issues that need to be resolved to improve the performance of activated carbons. With the exception of the surface functional groups involved in the adsorption of polar molecules, the specific interaction involved in the gas adsorbability of activated carbons has not been studied sufficiently. Smith et al. [13] conducted the first study on the comparison between benzene and cyclohexane adsorptions on graphite; in this study, stronger cyclohexane adsorption was observed than benzene adsorption. On the other hand, the strong $\pi$-electron interaction of benzene with nanopore surfaces was observed by Dosseh et al. [14]. Moreover, comparison studies on adsorbed molecules of $sp^2$ and $sp^3$ carbons have been conducted for benzene and cyclohexane and for ethylene and ethane [15–17]. The adsorption isotherms of ethane and ethylene on activated carbons showed larger amounts of adsorbed ethylene than ethane [18], indicating stronger interaction of $sp^2$ carbon with pore walls. Radovic and Bockrath used molecular orbital calculations to emphasise the essential importance of the conjugated $\pi$-electron nature of the basal plane of

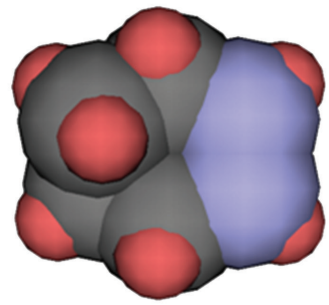

Figure 1: Space-filled model of cyclohexene. Blue, black, and red spheres represent $sp^2$ carbon atoms, $sp^3$ carbon atoms, and hydrogen atoms, respectively.

the graphite in the adsorption of organic molecules [19]. The characteristic interaction, the $\pi$-$\pi$ interaction of the $sp^2$ carbons in an adsorbed molecule with graphite, is caused by the electron cloud delocalization between the $sp^2$ carbons in the molecule and graphite. We still need to understand the difference between the adsorbed structures of the $sp^2$ and $sp^3$ carbon atoms of the adsorbate molecules upon adsorption on graphitic pores along with the dependence on pore width in order to obtain a better carbon adsorbent of high specificity for use in future technologies for the selective reaction and separation of unsaturated molecules. Vernov and Steele showed the orientation of adsorbed benzene on graphite using a 12-site model [20–22]. Do et al. studied the orientation structures of organic molecules on graphite and porous carbons using grand canonical Monte Carlo (GCMC) simulation, taking into account the molecular structures [23, 24]. Such molecular simulation studies can reveal the interactions between $sp^2$ carbon and a graphitic carbon surface along with the molecular structures.

Cyclic hydrocarbons are important intermediates in many chemical reactions on transition metal surfaces [25, 26]. Cyclohexene is one of the critical intermediates in catalytic reforming. Many studies on the reforming process have been reported [25–27]. The cyclohexene molecule has two $sp^2$ carbon atoms in addition to four $sp^3$ carbon atoms, making it an appropriate probe molecule for research on the comparison of the adsorptions of $sp^2$ and $sp^3$ carbon atoms. To understand the difference between the adsorbed structures of the $sp^2$ and $sp^3$ carbon atoms, we adopted GCMC simulation for studying cyclohexene adsorption on activated carbon. In addition, this study could serve as a guide in the development of better adsorption media for separating cyclohexene from commercial natural gas [4, 6, 15].

## 2. Simulation Procedures

Figure 1 shows a space-filled model of cyclohexene; the structural parameters are given in the paper by Faller et al. [28]. The cyclohexene molecule has a distorted plane structure that consists of five single bonds (C–C) and one double bond (C=C). The $sp^3$ and $sp^2$ carbon atoms must be distinguished by using interaction potential calculation and GCMC simulation. Faller et al. determine the parameters of cyclohexene for the flexible model [28]. As rigid and flexible models give no significant difference in structure [29, 30], a 16-centre model for the rigid cyclohexene structure in this study was adopted for the calculation ($\varepsilon/k_B$ = 31.9 K for H and 35.6 K for $sp^3$ and $sp^2$ carbons; $\sigma$ = 0.252 nm for H, 0.311 nm for $sp^3$ carbon, and 0.321 nm for $sp^2$ carbon) [28, 31]. The availability is verified by the comparison between the rigid and flexible models before the calculation; the assembly structures of cyclohexene in the rigid and flexible models are almost agreeing with each other, although the structure distribution in the flexible model is slightly dispersed due to the flexibility. The intermolecular interactions were described by the Lennard-Jones potentials:

$$\phi_{AB} = 4\sum_i \sum_j \varepsilon_{ij}\left[\left(\frac{\sigma_{ij}}{r_{ij}}\right)^{12} - \left(\frac{\sigma_{ij}}{r_{ij}}\right)^{6}\right]. \quad (1)$$

Here, $r_{ij}$ is the distance between the $i$th atom in molecule $A$ and the $j$th atom in molecule $B$. The Lorentz-Berthelot mixing rules were applied to obtain the interaction energy and size parameters for the heteroatomic interaction:

$$\sigma_{ij} = \frac{\sigma_i + \sigma_j}{2} \qquad \varepsilon_{ij} = \sqrt{\varepsilon_i \varepsilon_j}. \quad (2)$$

Here, each component atom in the molecule was assumed to be electrically neutral; the stable molecular geometry of a single molecule in the flexible model was used for the calculation.

The slit-shaped pore was modelled using the interface between two semi-infinite graphite slabs; the molecule-carbon wall interaction was approximated by the 10-4-3 Steele potential [32]:

$$\phi_{sf} = \sum_i A\left[\frac{2}{5}\left(\frac{\sigma_{sf_i}}{z_i}\right)^{10} - \left(\frac{\sigma_{sf_i}}{z_i}\right)^{4} - \frac{{\sigma_{sf_i}}^4}{1.005(z_i + 0.20435)^3}\right]. \quad (3)$$

Here, $A$ is 76.38 $\pi\varepsilon_{sfi}\sigma_{sfi}^2$, and $z$ is the vertical distance of the $i$th atom in a molecule from the centre of a carbon atom on one side of a carbon surface; $\sigma_{sfi}$ and $\varepsilon_{sfi}$ were derived from the Lorentz-Berthelot mixing rules. $\sigma_s$ and $\varepsilon_s$ are the Lennard-Jones parameters for the carbon atom in graphite ($\sigma_s$ = 0.3416 nm and $\varepsilon_s/k_B$ = 30.14 K), and $\sigma_{fi}$ and $\varepsilon_{fi}$ are the Lennard-Jones parameters for the $i$th atom in the molecule [33]. Strictly speaking, the molecule-graphite slab interaction was summed and smoothed by all of the interactions between the component atoms in the molecule and the graphite slab using the Steele potential. In the case of the graphite slit pore, the interaction of the cyclohexene molecule with the pore was expressed by the sum of the interaction potentials of the cyclohexene molecule with both graphite walls, as given by (4):

$$\phi_p = \phi_{sf}(z) + \phi_{sf}(H - z). \quad (4)$$

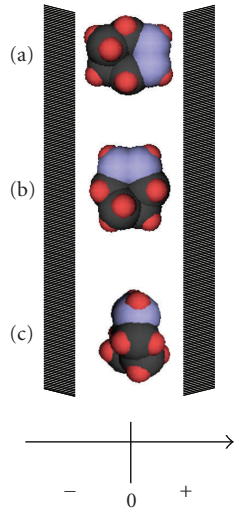


Figure 2: Molecular arrangements of adsorbed cyclohexene. Head-on (a), side-on (b), and in-plane (c) arrangements.

Here, $H$ is the physical slit pore width, which is the internuclear distance between opposite graphite walls. The physical slit pore width was associated with the pore width, $w$, which can be experimentally measured as follows [34]:

$$w = H - 2z_0, \quad z_0 = 0.856\ \sigma_{sf} - \frac{\sigma_{ff}}{2}. \tag{5}$$

Here, $z_0$ is the closest contact distance between the $sp^2$ carbon and the graphite pore wall.

The electrostatic interaction between a polar molecule and a graphitic slab must be taken into account for a detailed analysis of the adsorption of polar molecules, as reported in previous papers [20, 35]. The electrically neutral cyclohexene atoms assumed here nominally give no electrostatic contribution to the interaction between the cyclohexene and the pore wall. However, the electrostatic interaction is roughly included in the Lennard-Jones parameters obtained from the *ab initio* calculation by Faller et al. [28]. Grand canonical Monte Carlo simulations of the cyclohexene were performed using $3 \times 10^6$ steps at 298 K, with three equivalent trials for the creation, deletion, and movement of the molecules. The pressure was calculated from the bulk molecular density in the unit cell of $6 \times 6 \times 6\,nm^3$ by using the van der Waals equation after more than $1 \times 10^8$ calculation steps and the accumulation of $9 \times 10^7$ steps. A unit cell size of $6 \times 6 \times H\,nm^3$ and a 2-dimensional periodic boundary condition were used in this calculation.

## 3. Results and Discussion

The molecule-graphite pore interaction energy was calculated for three arrangements, as shown in Figure 2. The molecular plane is perpendicular to the graphite wall in arrangements (a) and (b). The double bond is head-on toward a plus-side wall for (a), whereas there is side-on adsorption on the wall for (b). Hence, (a) and (b) are called head-on and side-on arrangements, respectively. On the other hand, because the molecular plane is parallel to the wall in (c), arrangement (c) is called an in-plane configuration. The molecule-pore interaction potentials were calculated as a function of the vertical distance of the molecular centre of gravity from the pore centre for the three arrangements.

Figure 3 shows the molecule-pore interaction potentials for the three arrangements shown in Figure 2. For the smallest pore ($w = 0.6$ nm), the in-plane arrangement gets a large stabilization energy of −8000 K, suggesting the presence of adsorption from an extremely low pressure. The side-on arrangement provides the considerably large stabilization energy of −4000 K, whereas the head-on arrangement leads only to repulsive interaction energy. The potential profiles for $w = 0.7$ nm are remarkably different from those for $w = 0.6$ nm. The most stable arrangement (−7000 K) is found to be the side-on type with $w = 0.7$ nm. The in-plane arrangement gives double potential minima, and the head-on and side-on arrangements give a single minimum. All the potential minima are close to each other, within 500 K, for $w = 0.8$ nm. The head-on arrangement leads to the single deepest potential minimum for $w = 0.8$ nm, and the side-on and in-plane arrangements have double minima. In the case of $w > 0.9$ nm, the in-plane arrangement gave the deepest potential double minima, which are situated near the pore wall. Then, cyclohexene molecules on the pore walls will be adsorbed on the pore walls with $w > 0.9$ nm in the in-plane structure. Similar double potential minima were obtained for the side-on arrangement, and the depth was slightly shallower than that for the in-plane arrangement. It is worth noting that the head-on arrangement gave an asymmetrical potential profile for $w > 0.9$ nm; $sp^2$ carbon leads to a stronger interaction than $sp^3$ carbon. Even the single potential minima for $w = 0.7$ and 0.8 nm shift slightly in the positive direction due to the contribution by the $sp^2$ carbons (see Figures 3(b) and 3(c)). This interaction potential difference in the $sp^2$ and $sp^3$ carbon atoms is clearly observed in the adsorbed structure obtained from the GCMC simulation. The potential profiles for $w = 1.0$ nm have features that are almost similar to those for $w = 0.9$ nm (Figure 3(d)). Figure 4 shows the changes in the interaction potential minimum with the pore width for different adsorption structures. The interaction energy depends sensitively on the pore width and the molecular arrangement in the pore; the most favourable arrangement predicted from the interaction potential varies with the pore width. The deepest potential energy is obtained in the in-plane arrangement for $w < 0.64$ nm. The side-on arrangement provides the deepest potential energy in the $w$ range of 0.64 to 0.75 nm. The head-on arrangement gives the deepest interaction potential energy for $w = 0.75$–$0.84$ nm, indicating a contribution by the $sp^2$ carbon atoms in the pores when $w$ is approximately 0.8 nm, although the energy difference from the side-on arrangement is not marked compared with the difference for smaller pores.

Figure 5 shows the adsorption isotherms of cyclohexene in pores with $w = 0.5$–$2.0$ nm at 298 K. The ordinate represents the number of cyclohexene molecules adsorbed in the pore, with wider pores resulting in larger numbers of molecules above $10^{-5}$ MPa. As the pore with $w = 0.5$ nm is

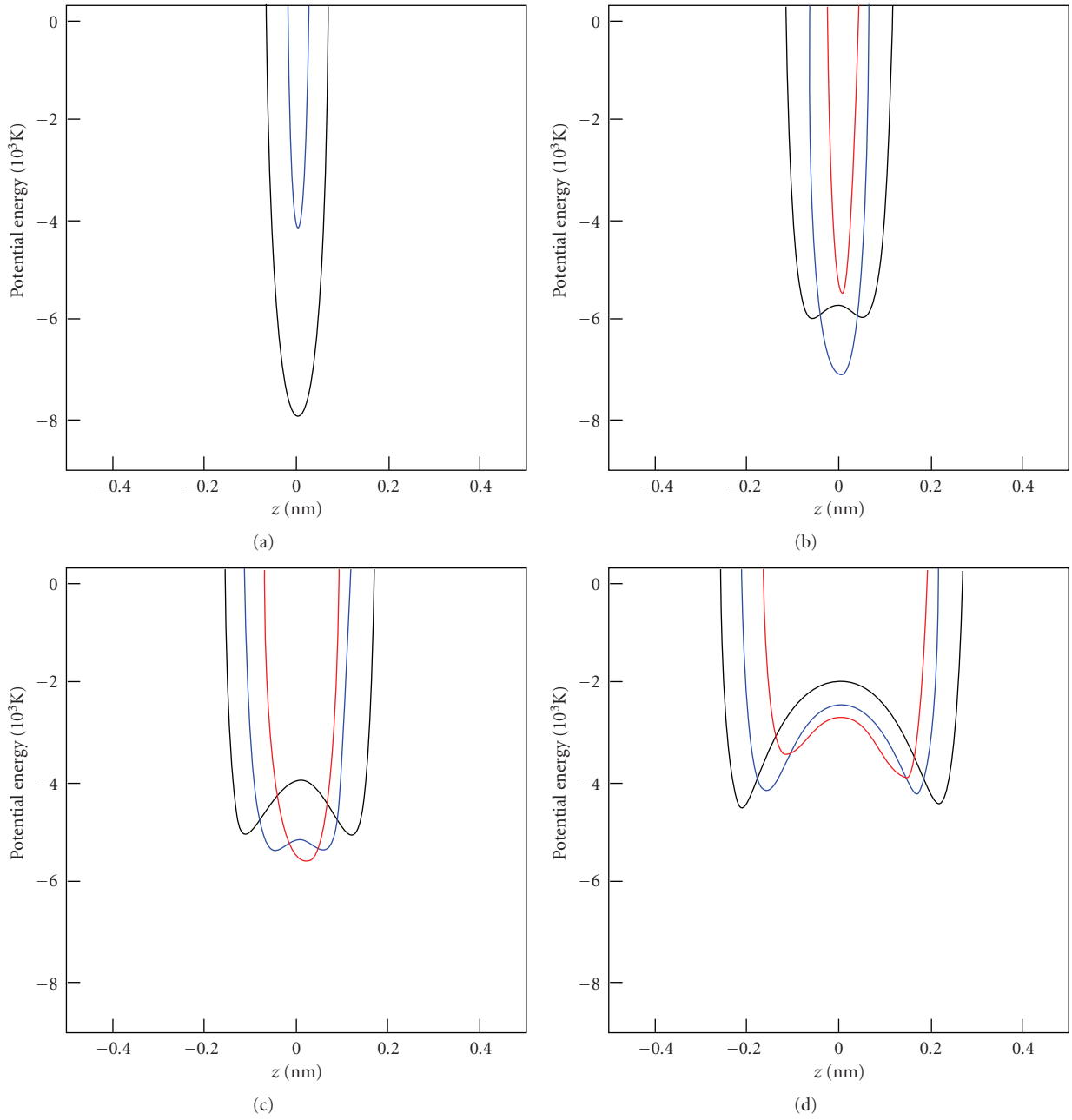


FIGURE 3: Potential profiles of a cyclohexene molecule in graphitic slit pores with $w = 0.6$ (a), 0.7 (b), 0.8 (c), and 1.0 nm (d). Red curve: head-on arrangement, blue curve: side-on arrangement, and black curve: in-plane arrangements.

too narrow to accommodate cyclohexene molecules easily, adsorption begins above $10^{-8}$ MPa. On the other hand, the pore with $w = 0.6$ nm, which has the deepest potential minimum (−8000 K) for the in-plane arrangement, exhibits a quite intensive adsorption for cyclohexene; this adsorption begins even below $10^{-10}$ MPa. As the pore with $w = 1.0$ nm has double minima, which are in the range from −4000 to −4500 K, adsorption begins at $5 \times 10^{-9}$ MPa. The adsorption for $w > 1.0$ nm begins above $5 \times 10^{-9}$ MPa. The cyclohexene molecule has a distorted ring structure, making dense packing in a smaller slit pore space very difficult. This can be understood from the following snapshot analysis.

Figure 6 shows the snapshots at $10^{-3}$ MPa for $w = 0.6$, 0.7, 0.8, and 1.0 nm. Cyclohexene molecules form a single adsorbed layer that is inherent to the pore width for $w = 0.6$–0.8 nm, as shown in Figure 4. In the pore with $w = 0.6$ nm, the cyclohexene molecules basically exhibit the in-plane arrangement. Strictly speaking, the cyclohexene molecules are tilted against the pore wall due to the stronger $sp^2$ carbon-pore wall interaction. The tilt angle will be shown

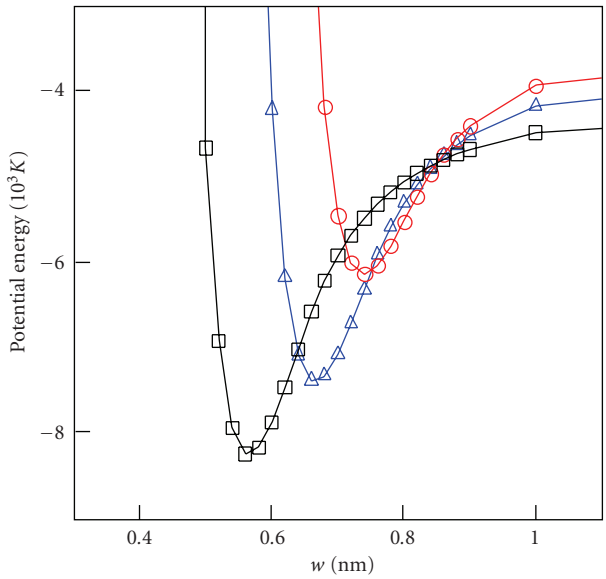


FIGURE 4: Potential minima as function of pore width. ◯: head-on arrangement, △: side-on arrangement, and □: in-plane arrangements.

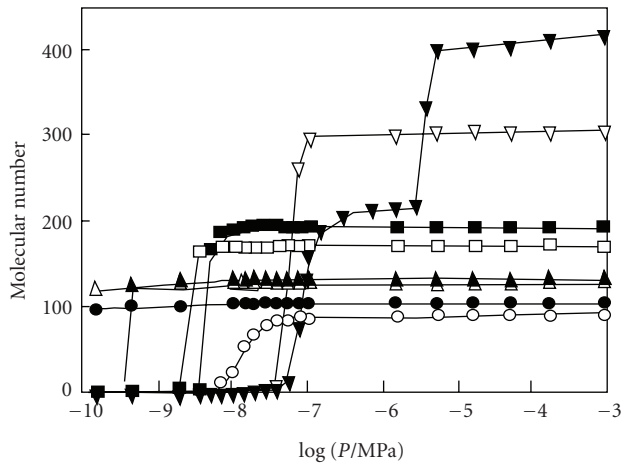


FIGURE 5: Adsorption isotherms of cyclohexene at 298 K. ◯: $w$ = 0.5 nm, •: $w$ = 0.6 nm, △: $w$ = 0.7 nm, ▲: $w$ = 0.8 nm, □: $w$ = 0.9 nm, ■: $w$ = 1.0 nm, ▽: $w$ = 1.5 nm, and ▼: $w$ = 2.0 nm.

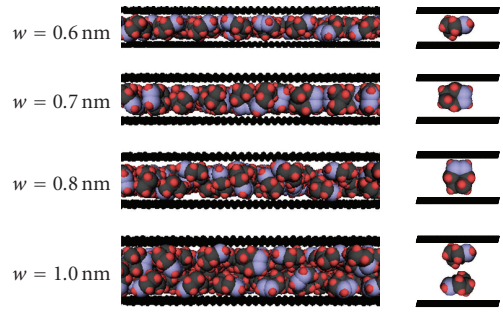


FIGURE 6: Snapshots of adsorbed cyclohexene in the nanopores with $w$ = 0.6, 0.7, 0.8, and 1.0 nm at $P = 10^{-3}$ MPa. Right side: schematic model of typical structure of adsorbed cyclohexene. Blue, grey, and red spheres depict $sp^2$ carbon, $sp^3$ carbon, and hydrogen, respectively. Graphitic carbon walls are represented by the loose lines composed of black spheres.

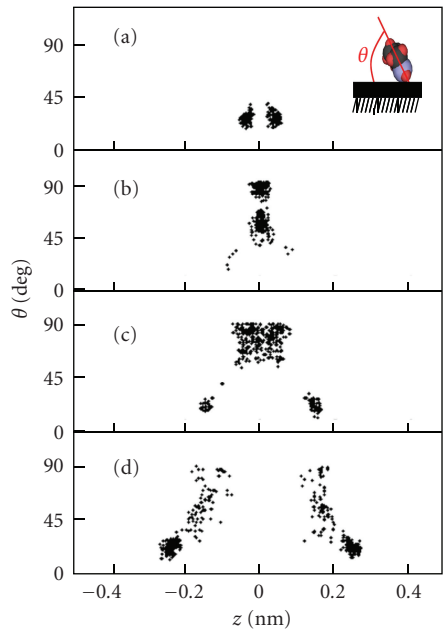


FIGURE 7: Angular distribution of cyclohexene against the plane of the pore wall of $w$ = 0.6 (a), 0.7 (b), 0.8 (c), and 1.0 nm (d).

later. Single adsorbed layers having the side-on and head-on arrangements are observed in the pores with $w$ = 0.7 and 0.8 nm, respectively, which is expected from the results shown in Figure 4. Two adsorbed layers of cyclohexene molecules are formed in the pore with $w$ = 1.0 nm. Three layers and four layers are observed in the pores with $w$ = 1.5 and 2.0 nm, respectively, which are not shown in this paper. In the case of the pores with $w$ = 1.5 and 2.0 nm, molecules at the monolayer position orientate along the pore walls; molecules in the central space of the pore have almost a perpendicular configuration against the pore wall with less molecular orientation.

The tilting of the cyclohexene molecules toward the pore walls clearly shows the molecular orientation to a pore wall. Figure 7 shows the angular distribution between the normal vector of a cyclohexene molecule and the pore wall surface. Here, the normal vector is defined as a perpendicular vector to the plane of two $sp^2$ carbons and two $sp^3$ carbons next to the $sp^2$ carbon; that is, the in-plane arrangement is at 0° and the head-on or side-on arrangement is at 90°. The probable angles for $w$ = 0.6 and 0.7 nm are 20–30° and 50–90°, respectively. Thus, the in-plane arrangement is expected for $w$ = 0.6 nm, while the head-on or side-on arrangement should be formed in the pore with $w$ = 0.7 nm. For $w$ = 0.8 and 1.0 nm, angles of 20–30° are observed in the contacts with the pore walls. Angle distributions above 50° are also observed at some pore-centred positions, suggesting the head-on or side-on arrangement. The head-on or side-on arrangement is mainly formed for $w$ = 0.8 nm. On the other

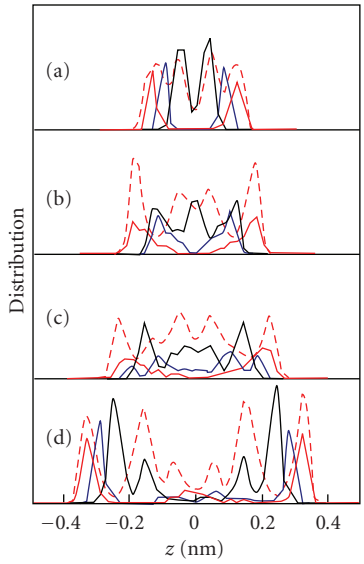


Figure 8: Distributions of cyclohexene in a direction perpendicular to the pore wall at $10^{-3}$ MPa, for $w = 0.6$ (a), 0.7 (b), 0.8 (c), and 1.0 nm (d). Black curve: $sp^3$ carbon, blue curve: $sp^2$ carbon, red solid curve: hydrogen bound to $sp^2$ carbon, and red dashed curve: hydrogen bound to $sp^3$ carbon.

hand, the in-plane arrangement is the most common for $w = 1.0$ nm.

As the exact arrangement of the molecules facing the pore wall can provide useful information on the role of the $sp^2$ carbon atoms in the molecule-pore wall interaction, distribution profiles were determined for the $sp^2$ and $sp^3$ carbons in the adsorbed cyclohexene against the perpendicular axis of the pore walls, as shown in Figure 8. The snapshots in Figure 6 and angular distribution in Figure 7 cannot provide a clear insight into the role of the $sp^2$ carbon atoms in the cyclohexene-pore wall interaction. Cruz and Mota found a slight difference between the distances of the $sp^2$ and $sp^3$ carbons from pore walls [16]. In contrast, Figure 8 distinctly shows the difference in the positions of the $sp^2$ and $sp^3$ carbon atoms and the hydrogen atoms bonding to the $sp^2$ and $sp^3$ carbons. The $sp^2$ carbon atoms are actually in contact with a pore wall for $w = 0.6$ and 1.0 nm, although the remarkable difference between the $sp^2$ and $sp^3$ carbon atoms near the walls is not observed well for $w = 0.7$ and 0.8 nm. The $sp^2$ carbon has a considerably uniform distribution for $w = 0.8$ nm, and a few $sp^2$ carbons are closer to the wall than the $sp^3$ carbon, whereas the $sp^3$ carbon prefers the monolayer position. The distributions for $w = 1.5$ and 2.0 nm had tendencies similar to that for $w = 1.0$ nm; these distributions for $w > 1.0$ nm have sharp peaks near the pore walls, and no clear peak exists at around the centre of the pore. The distribution peak of the $sp^2$ carbon is closer to the pore walls than that of the $sp^3$carbon atoms for $w = 0.6$, 1.0, 1.5, and 2.0 nm, despite the fact that the Lennard-Jones diameter of the $sp^2$ carbon is larger than that of the $sp^3$ carbon by 0.01 nm. Therefore, the $sp^2$ carbon atoms can interact preferentially with the graphite walls in comparison with the interaction of the $sp^3$ carbon atoms for the specific pore widths. The hydrogen atoms bound to the $sp^2$ carbons are also distributed on the pore walls, whereas those bound to the $sp^3$ carbons are orderly distributed in the pores. In comparison to the carbon atoms, there exist nearer hydrogen atoms to the pore walls.

## 4. Conclusion

The preferential interaction of $sp^2$ carbon atoms with a graphite wall is explicitly observed in the adsorption of cyclohexene in graphite slit pores, with the exception of pores with $w = 0.7$ and 0.8 nm, as cyclohexene has both $sp^2$ and $sp^3$ carbon atoms. The preferential interactions of the $sp^2$ carbon atoms and the hydrogen atoms bound to the $sp^2$ carbon atoms in cyclohexene are enhanced in a restricted nanoscale pore space; this results in cyclohexene having a slightly tilted conformation. The application of the preferential interaction nature of the $sp^2$ carbon atoms to the design of a better adsorbent for aromatic compounds is expected to be quite useful, because the orientation of cyclohexene to the graphite walls depends on the pore width.

## Acknowledgments

The financial support provided by the Kurata Memorial Hitachi Science and Technology Foundation, Kurita Water and Environment Foundation, Nippon Sheet Glass Foundation, and Global COE program, MEXT, Japan, is gratefully acknowledged.

## References

[1] K. Kaneko, C. Ishii, M. Ruike, and H. kuwabara, "Origin of superhigh surface area and microcrystalline graphitic structures of activated carbons," *Carbon*, vol. 30, no. 7, pp. 1075–1088, 1992.

[2] T. Ohba, D. Nicholson, and K. Kaneko, "Temperature dependence of micropore filling of N in slit-shaped carbon micropores: experiment and grand canonical Monte Carlo simulation," *Langmuir*, vol. 19, no. 14, pp. 5700–5707, 2003.

[3] J. Laine and S. Yunes, "Effect of the preparation method on the pore size distribution of activated carbon from coconut shell," *Carbon*, vol. 30, no. 4, pp. 601–604, 1992.

[4] M. M. A. Freitas and J. L. Figueiredo, "Preparation of carbon molecular sieves for gas separations by modification of the pore sizes of activated carbons," *Fuel*, vol. 80, no. 1, pp. 1–6, 2001.

[5] K. Gergova and S. Eser, "Effects of activation method on the pore structure of activated carbons from apricot stones," *Carbon*, vol. 34, no. 7, pp. 879–888, 1996.

[6] T. J. Bandosz, "Effect of pore structure and surface chemistry of virgin activated carbons on removal of hydrogen sulfide," *Carbon*, vol. 37, no. 3, pp. 483–491, 1999.

[7] T. Kyotani, "Control of pore structure in carbon," *Carbon*, vol. 38, no. 2, pp. 269–286, 2000.

[8] D. Qu and H. Shi, "Studies of activated carbons used in double-layer capacitors," *Journal of Power Sources*, vol. 74, no. 1, pp. 99–107, 1998.

[9] E. Frackowiak and F. Béguin, "Electrochemical storage of energy in carbon nanotubes and nanostructured carbons," *Carbon*, vol. 40, no. 10, pp. 1775–1787, 2002.
[10] P. Simon and Y. Gogotsi, "Materials for electrochemical capacitors," *Nature Materials*, vol. 7, no. 11, pp. 845–854, 2008.
[11] F. Dreisbach, R. Staudt, and J. U. Keller, "High pressure adsorption data of methane, nitrogen, carbon dioxide and their binary and ternary mixtures on activated carbon," *Adsorption*, vol. 5, no. 3, pp. 215–227, 1999.
[12] M. Sudibandriyo, Z. Pan, J. E. Fitzgerald, R. L. Robinson, and K. A. M. Gasem, "Adsorption of methane, nitrogen, carbon dioxide, and their binary mixtures on dry activated carbon at 318.2 K and pressures up to 13.6 MPa," *Langmuir*, vol. 19, no. 13, pp. 5323–5331, 2003.
[13] R. N. Smith, C. Pierce, and H. Cordes, "Adsorption of benzene and cyclohexane by graphite," *Journal of the American Chemical Society*, vol. 72, no. 12, pp. 5595–5597, 1950.
[14] G. Dosseh, Y. Xia, and C. Alba-Simionesco, "Cyclohexane and benzene confined in MCM-41 and SBA-15: confinement effects on freezing and melting," *Journal of Physical Chemistry B*, vol. 107, no. 26, pp. 6445–6453, 2003.
[15] S. Curbelo and E. A. Müller, "Modelling of ethane/ethylene separation using microporous carbon," *Adsorption Science and Technology*, vol. 23, no. 10, pp. 855–865, 2005.
[16] F. J. A. L. Cruz and J. P. B. Mota, "Thermodynamics of adsorption of light alkanes and alkenes in single-walled carbon nanotube bundles," *Physical Review B*, vol. 79, no. 16, Article ID 165426, 2009.
[17] T. R. Rybolt, C. E. Wells, C. R. Sisson, C. B. Black, and K. A. Ziegler, "Evaluation of molecular mechanics calculated binding energies for isolated and monolayer organic molecules on graphite," *Journal of Colloid and Interface Science*, vol. 314, no. 2, pp. 434–445, 2007.
[18] B. U. Choi, D. K. Choi, Y. W. Lee, B. K. Lee, and S. H. Kim, "Adsorption equilibria of methane, ethane, ethylene, nitrogen, and hydrogen onto activated carbon," *Journal of Chemical and Engineering Data*, vol. 48, no. 3, pp. 603–607, 2003.
[19] L. R. Radovic and B. Bockrath, "On the chemical nature of graphene edges: origin of stability and potential for magnetism in carbon materials," *Journal of the American Chemical Society*, vol. 127, no. 16, pp. 5917–5927, 2005.
[20] A. Vernov and W. A. Steele, "The electrostatic field at a graphite surface and its effect on molecule-solid interactions," *Langmuir*, vol. 8, no. 1, pp. 155–159, 1992.
[21] A. Vernov and W. A. Steele, "Computer simulations of benzene adsorbed on graphite. 2. 298 k," *Langmuir*, vol. 7, no. 11, pp. 2817–2820, 1991.
[22] A. Vernov and W. A. Steele, "Computer simulations of benzene adsorbed on graphite. 1. 85 K," *Langmuir*, vol. 7, no. 12, pp. 3110–3117, 1991.
[23] D. D. Do and H. D. Do, "Adsorption of carbon tetrachloride on graphitized thermal carbon black and in slit graphitic pores: five-site versus one-site potential models," *Journal of Physical Chemistry B*, vol. 110, no. 19, pp. 9520–9528, 2006.
[24] D. D. Do and H. D. Do, "Adsorption of ethylene on graphitized thermal carbon black and in slit pores: a computer simulation study," *Langmuir*, vol. 20, no. 17, pp. 7103–7116, 2004.
[25] M. Saeys, M. F. Reyniers, M. Neurock, and G. B. Marin, "Adsorption of cyclohexadiene, cyclohexene and cyclohexane on Pt(1 1 1)," *Surface Science*, vol. 600, no. 16, pp. 3121–3134, 2006.
[26] C. Papp, R. Denecke, and H. P. Steinrück, "Adsorption and reaction of cyclohexene on a Ni(111) surface," *Langmuir*, vol. 23, no. 10, pp. 5541–5547, 2007.
[27] W. G. Xu, Z. F. Shang, and G. C. Wang, "Adsorption of cyclohexene on nAu/Pt(1 0 0) (n = 0, 1, 2): a DFT study," *Journal of Molecular Structure: THEOCHEM*, vol. 869, no. 1–3, pp. 47–52, 2008.
[28] R. Faller, H. Schmitz, O. Biermann, and F. Müller-Plathe, "Automatic parameterization of force fields for liquids by simplex optimization," *Journal of Computational Chemistry*, vol. 20, no. 10, pp. 1009–1017, 1999.
[29] G. Cardini, "A comparison between the rigid and flexible model of cyclohexane in the plastic phase by molecular dynamic simulations," *Chemical Physics*, vol. 193, no. 1-2, pp. 101–108, 1995.
[30] I. G. Tironi, R. M. Brunne, and W. F. Van Gunsteren, "On the relative merits of flexible versus rigid models for use in computer simulations of molecular liquids," *Chemical Physics Letters*, vol. 250, no. 1, pp. 19–24, 1996.
[31] H. Schmitz, R. Faller, and F. Müller-Plathe, "Molecular mobility in cyclic hydrocarbons: a simulation study," *Journal of Physical Chemistry B*, vol. 103, no. 44, pp. 9731–9737, 1999.
[32] W. A. Steele, "The physical interaction of gases with crystalline solids. I: gas-solid energies and properties of isolated adsorbed atoms," *Surface Science*, vol. 36, no. 1, pp. 317–352, 1973.
[33] Y. F. Yin, B. McEnaney, and T. J. Mays, "Dependence of GCEMC simulations of nitrogen adsorption on activated carbons on input parameters," *Carbon*, vol. 36, no. 10, pp. 1425–1432, 1998.
[34] K. Kaneko, R. F. Cracknell, and D. Nicholson, "Nitrogen adsorption in slit pores at ambient temperatures: comparison of simulation and experiment," *Langmuir*, vol. 10, no. 12, pp. 4606–4609, 1994.
[35] X. Zhao and J. K. Johnson, "An effective potential for adsorption of polar molecules on graphite," *Molecular Simulation*, vol. 31, no. 1, pp. 1–10, 2005.